

Evaluation and Analysis of Microwave Flex Resonators designed to induce the spin-flip in the Positrons within the Antihydrogen atoms trapped at the ALPHA apparatus

Themis Coral Ovando Villegas

Universidad Privada Boliviana, Cochabamba, Bolivia

Abstract

The absence of antimatter, the counterpart to matter, represents one of the most profound mysteries in modern physics and is the subject of extensive research at CERN (the European Organization for Nuclear Research). A leading experiment in this field is ALPHA (Antihydrogen Laser Physics Apparatus), which aims to study the properties of antihydrogen, the antimatter equivalent of hydrogen. A significant achievement of the ALPHA experiment has been the observation of resonant quantum transitions in trapped antihydrogen. To take measurements further, a precise and accurate flexible microwave resonator is required to induce spin flips in the antiprotons within the antihydrogen atoms.

As part of this effort, thirteen different microwave resonators were designed and fabricated. In this way, this project focuses on the design and implementation of tools to analyse and evaluate the performance of these resonators. Additionally, the project includes a thorough analysis and interpretation of the results, contributing to the refinement of the experimental techniques used to study antihydrogen.

Keywords

Antimatter; ALPHA; Resonant quantum transitions; Microwave Resonator.

1 Introduction

1.1 Antimatter

In the beginning of the universe, during the Big Bang, both matter and antimatter were created in equal amounts. But somehow, at present, matter dominates our reality. This discrepancy presents one of the most profound mysteries in modern physics: What happened to the antimatter? Where does this asymmetry come from?

Antimatter is just the counterpart of matter. As regular matter is composed of particles, antimatter is composed of antiparticles. These antiparticles share the same mass as their corresponding matter particles but exhibit opposite properties, such as electric charge. For example, the positron is the antiparticle of the electron, possessing the same mass but a positive charge, as opposed to the electron's negative charge.

When matter and antimatter come into contact, they annihilate each other in a burst of energy. In this context, this process theoretically should have resulted in the mutual destruction of both matter and antimatter in the early universe and left it solely with radiation. However, due to an unknown mechanism that caused a slight imbalance, a small excess of matter survived, leading to the matter-dominated universe we observe today.

The study of antimatter continues to be a key area of research, with implications for developing different potential applications in fields like medical imaging and energy production. Furthermore, understanding the behaviour and interactions of antimatter is crucial in unravelling the mystery of this imbalance and the nature of our universe [1-2].

1.2 ALPHA

ALPHA (Antihydrogen Laser Physics Apparatus) is an international collaboration settled at CERN (European Centre for Nuclear Investigation) that aims to understand the fundamental properties of antimatter, particularly antihydrogen. It is also known as the Antimatter Factory given that is the only place on Earth where antimatter is created and trapped. In specific, by trapping antihydrogen atoms in a magnetic field, scientists in ALPHA can perform precise measurements to test the symmetry between matter and antimatter and various experiments with antimatter. The projects and experiments carried out here are crucial for advancing our understanding of fundamental physics, particularly in testing the principles of CPT symmetry (Charge, Parity, and Time reversal) and exploring why the universe contains more matter than antimatter.

The experimental cycle at ALPHA begins with the production of antiprotons and positrons, which are the antimatter counterparts of protons and electrons, respectively. Antiprotons are obtained from CERN's Antiproton Decelerator (AD), a machine that produces low-energy antiprotons. While positrons are sourced from a sodium-22 radioactive source and slowed down at the Positron Source and the Positron Accumulator. These particles are then trapped separately using Penning traps, which are devices that employ a combination of magnetic and electric fields to confine charged particles in a controlled environment.

At the same time, cooling and compressing the particles is a critical step, achieved through techniques like electron cooling and evaporative cooling, which reduce the particles' kinetic energy and prepare them for the next stages of the experiment. Once the antiprotons and positrons are sufficiently cooled and compressed, they are carefully mixed in a neutral environment within a specialized atom trap to synthesize antihydrogen atoms. This mixing process is delicate and requires precise conditions to ensure that the antihydrogen atoms are formed and remain stable.

The synthesized antihydrogen atoms are then trapped in a magnetic field using a device called an Ioffe-Pritchard trap. This magnetic trap is essential for keeping the antihydrogen atoms isolated from regular matter, preventing them from annihilating. With the antihydrogen atoms securely trapped, researchers can begin conducting experiments to study their properties.

Using lasers and microwaves, they can measure the response of antihydrogen to these stimuli, providing insights into its energy levels and magnetic properties. After the experiments, the antihydrogen is released from the trap, and the remnants are analysed to gather further data [2-4].

1.2.1 Resonant quantum transitions in trapped antihydrogen atoms

At ALPHA, one of the pivotal experiments aimed at testing CPT symmetry (charge conjugation, parity, and time reversal) focuses on resonant quantum transitions in antihydrogen. This experiment specifically investigates the spin-flipping of positrons within antihydrogen atoms, a process critical for high-precision measurements of antihydrogen's properties. By using resonant microwave radiation, researchers successfully manipulated the internal spin state of antihydrogen atoms. This manipulation led to variations in the survival rates of antihydrogen, depending on whether the microwaves were on or off resonance. The observed differences in survival ratios underscore the sensitivity of antihydrogen to resonant conditions, highlighting the experiment's capability to probe fundamental symmetries.

Building on this effort, the spin-flipping of antiprotons within antihydrogen atoms has also been proposed. Achieving this requires the designing and engineering of a specialized microwave cavity resonator with a resonance frequency tailored to induce spin flips in antiprotons. This resonator will be integrated into a specific electrode within the Penning trap that confines the antihydrogen atoms. In this way, the successful development of this resonator is expected to contribute to the advancing of our understanding of antimatter and further extend the frontiers of modern physics [5].

1.2.2 Penning Trap

A Penning trap is a device used in physics to confine charged particles using a combination of electric and magnetic fields. It is essential in experiments that involve the manipulation of particles like ions or electrons, including antimatter research. The trap works by applying a solenoidal magnetic field along its axis, which causes charged particles to spiral around the magnetic field lines due to the Lorentz force. This spiral motion confines the particles radially, while a quadratic electric potential generated by voltages on electrodes confines them axially, preventing them from escaping the trap.

In the ALPHA experiment, a variation called the Penning-Malmberg trap is employed. Unlike the ideal Penning trap, where electric potentials are perfectly quadratic, the Penning-Malmberg trap uses a more practical setup with cylindrical electrodes. This configuration, though not perfectly quadratic, is highly effective in confining charged plasmas like positrons, antiprotons, and electrons. The particles within the trap emit cyclotron radiation as they spiral, which helps cool them and stabilize their motion.

In this way, a penning trap allows scientists to isolate and manipulate charged particles before they combine into neutral antihydrogen atoms, which cannot be confined by the same means. This precise control over charged plays an important role in the studying of antimatter and conducting experiments in plasma physics [6].

2 Project development process

In the context of the design of a resonator to induce antiprotons' spin flip within the antihydrogen atom, a series of models with varying geometric parameters were developed. Distinct resonator designs were fabricated and tested using a Vector Network Analyzer (VNA). The analysis focused on key performance metrics, including S-parameters, resonance frequency, and quality factors. To achieve this, two custom software were created to process the data and enable a comprehensive comparison with theoretical predictions and facilitating detailed analysis.

As previously stated, various models with distinct geometric parameters were designed, simulated, and fabricated. Specifically, the parameters varied in these designs were:

- Length (L)
- Distance between the resonator and the feeding lines (D)
- Width of the feeding lines (PW)
- Length of the feeding lines (PL)

A detailed visual schematic of these parameters was created for a better spatial understanding of them.

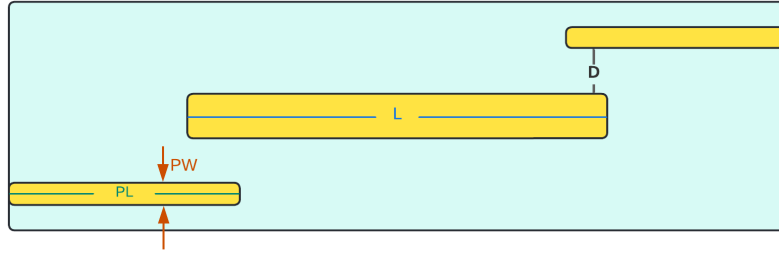


Fig. 1 Resonator's geometric parameters (L, D, PW, PL)

The resonators, each featuring a unique combination of design parameters, were fabricated and printed by an external company to explore a broad parameter space. For instance, the first resonator was designed with dimensions of $L = 131.5$ mm, $D = 0.05$ mm, $PW = 0.3$ mm, $PL = 70$ mm, and included a distinctive uncovered centre, differing from the standard flex resonators used in other samples. This variation aimed to assess its impact on the resonator's electromagnetic properties, particularly its resonance behaviour.

To ensure accurate analysis, the following steps were carried out taken into account Pozar's recommendations from his book *Microwave Engineering*. In this way, each resonator was equipped with SMA connectors, which were meticulously soldered to both ends. This setup was critical for minimizing signal loss and achieving accurate impedance matching. According to this book, proper impedance matching is essential to prevent signal reflection and ensure reliable measurement of the resonator's characteristics [7].

For the measurements, a Vector Network Analyzer (VNA) was employed. The VNA used was the Keysight PNA Network Analyzer, model N5224B, which covers a broad frequency range from 900 Hz to 43.5 GHz. This range is particularly suited for high-frequency resonator analysis.

Before each data collection session, the VNA was carefully calibrated for both ports to ensure measurement integrity. Calibration procedures were crucial for eliminating systematic errors and ensuring the accuracy of the S-parameter measurements. Following calibration, S-parameter measurements were conducted on each resonator. The resulting data, including both the S-parameters in ".csv" format and real-time screenshots of the VNA's plots, were saved and exported for further analysis. This comprehensive approach ensured that both numerical and visual data representations of the resonators' performance were captured and could be thoroughly evaluated [7].



Fig. 2 VNA calibration

Following data acquisition, a thorough analysis was performed using custom software developed in Python. This first application was specifically designed to handle various analytical tasks based on the VNA resonator data, providing a comprehensive suite of features:

- Plot S-parameters
- Measure and display the loaded and unloaded quality factor
- Measure and display the coupling factor
- Display the lower and higher cut-off frequency used to calculate the bandwidth, which was used to calculate the quality factor
- Plot the Impedance (Z) and Admittance (Y) parameters
- Apply a low-pass filter to the selected S-parameters to filter the signal approximation from the noise
- Measure and display on the graph the resonance frequency in a message box
- Measure and display on the graph the filtered resonance frequency in a message box

The application supports detailed report generation and the ability to save graphical outputs according to user-defined conditions. Users can customize their analysis by selecting from multiple options to tailor the software's output to specific needs. A screenshot of the interface, analysing an example dataset, is included in figure 3 to illustrate the software's capabilities.



Fig. 3 First resonator's analysis ($L = 131.5$ mm, $D = 0.05$ mm, $PW = 0.3$ mm, $PL = 70$ mm) with the “Resonator’s Analyzer and Plotter” (Software 1)

Furthermore, the software supports the integration of simulation data, allowing users to upload theoretical models and overlay them with experimental VNA data for direct visual comparison. This feature facilitates the validation of theoretical predictions against empirical results. The software also enables the generation of summarized reports applicable for both experimental and simulated data. These reports take into account user-adjustable parameters, such as L , D , PW , and PL , along with calculated metrics, including resonance frequency, loaded and unloaded quality factors, and the coupling factor.

Once this software was ready, each resonator was individually analysed with this tool. Hence, thirteen different reports were generated and evaluated for both the simulated and experimental data. Then, to take this analysis further, a second software application was developed.

This second software was a “Reports’ Analyzer”. It is able to read reports in batches generated with the first software and, based on these, plot statistics in graphs which are based on different parameters. Specifically, there are two columns, right and left side, on the first column the following parameters are displayed as checkboxes:

- QL (Loaded Quality factor)
- Q0 (Unloaded Quality factor)
- Coupling Factor
- Resonance frequency
- Filtered resonance frequency

And on the right side:

- L
- D
- PW
- PL

Each acronym stands for the previously specified resonator's geometric parameter.

To upload reports in this second application, the users can either drag and drop from their files or use a dedicated button for so. Additionally, it displays a table in which all the reports' results are visually displayed. As shown in the following screenshot (Fig. 4).

L (mm)	D (mm)	PW (mm)	PL (mm)	Res. Freq. (MHz)	Res. Mag.	Filt. Res. Freq.	Filt. Res. Mag.	Coupling	Coupling dB	QL	Q0	QE	Lower Cutoff	Upper Cutoff	Cutoff
131.5	0.05	0.3	70	593601000.0	-55.7	593601000.0	-58.4	0.001197	-58.43	10.12	10.13	8461.84	565643000.00	624296000.00	-61.4
127.5	0.05	0.3	70	658925000.0	-52.6	658925000.0	-55.4	0.001709	-55.34	11.00	11.02	6448.33	631093000.00	690971000.00	-58.2
122.5	0.05	0.3	75	687240000.0	-51.1	687240000.0	-53.5	0.002123	-53.46	11.37	11.40	5366.43	658610000.00	719048000.00	-56.4
122.5	0.06	0.3	70	688122000.0	-57.0	688122000.0	-60.0	0.000995	-60.04	10.83	10.84	10892.18	659604000.00	723136000.00	-63.1
122.5	0.05	0.4	70	686407000.0	-56.5	686407000.0	-59.4	0.001071	-59.41	10.99	11.00	10276.36	657742000.00	720189000.00	-62.4

Fig. 4 “Resonators’ Reports’ Analyzer” software

Some samples of the graphs it can plot include Resonance Frequency vs L, Coupling Factor vs D, and many others.

It is also notable that it can distinguish the simulated from the experimental data. For this to be possible, a string ‘simulation’ should externally be included at the end of any simulation report.

3 Resonators’ evaluation and results

During the initial evaluation of the resonators, seven were excluded from further analysis due to excessive noise and the absence of a notable resonance frequency. The geometric parameters and evaluation are schemed in Table 1.

Table 1: First sample of resonators undergone evaluation

L	D	PW	PL	Acceptable and noticeable Resonance Frequency?	NOISE?
131.5	0.05	0.3	70	Yes	No
127.5	0.05	0.3	70	Yes	No
125	0.05	0.3	70	No	Yes
122.5	0.08	0.3	70	Yes	Yes
122.5	0.06	0.3	70	Yes	No
122.5	0.05	0.9	70	Yes	Yes
122.5	0.05	0.6	70	Yes	No
122.5	0.05	0.4	70	Yes	No
122.5	0.05	0.3	75	Yes	No
122.5	0.05	0.3	70	Yes	Yes
122.5	0.05	0.3	65	Yes	No
122.5	0.1	0.3	70	Yes	Yes
120	0.05	0.3	70	No	Yes

Subsequent evaluations and discussions within the Microwave ALPHA team regarding the resonators' S-parameters and frequency responses led to the further exclusion of additional resonators. For the final evaluation, a selection criterion was established based on the S21 parameter graphs and the quality factor of each resonator. The primary objective was to identify resonators with a clear resonance frequency and minimal noise levels in the S21 graphs to ensure accurate characterization. Additionally, both the loaded and unloaded quality factors were required to be at least 10. This threshold was set because resonators with a low-quality factor tend to exhibit significant energy dissipation or are more susceptible to external interference, resulting in broadened resonance peaks and increased noise levels in the S-parameter data. Such conditions can obscure the true resonance characteristics and compromise data reliability for subsequent analyses. Consequently, resonators that did not meet this quality factor criterion were excluded from the final evaluation.

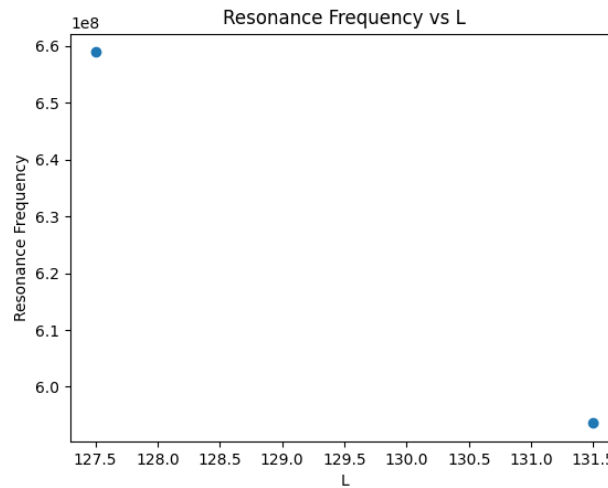
As a result, out of the 13 resonators tested, only 5 met these stringent criteria. Consequently, the scope of subsequent measurements and parameter isolation was somewhat constrained. Table 2 provides details of the selected resonators, including their resonance frequency, observed noise levels, and loaded quality factor. Emphasis was placed on the loaded quality factor, as it reflects both internal losses and external loading effects.

Table 2: Final sample of resonators undergone evaluation

L	D	PW	PL	Acceptable and noticeable Resonance Frequency?	Noise?	Loaded Quality Factor
131.5	0.05	0.3	70	Yes	No	10.12
127.5	0.05	0.3	70	Yes	No	11
122.5	0.06	0.3	70	Yes	No	10.83
122.5	0.05	0.4	70	Yes	No	10.99
122.5	0.05	0.3	75	Yes	No	11.37

Then, the resonators listed in this table were initially assessed individually using the first software, “Resonator’s Analyzer and Plotter” and later in a batch with the “Reports’ Analyzer”. Detailed graphs of the experimental S21 and S22 parameters, as well as filtered parameters for each resonator, are available in Appendix A. Each graph includes a message box that visually indicates the resonance frequency.

Subsequently, the second software, Resonators’ Reader and Analyzer, was employed to further analyse the resonators. Specifically, the first two resonators from table 2 were selected for plotting the length (L) against resonance frequency. This decision was due to their common values for D, PW, and PL, with the sole variable being their length (L). This approach allowed for a focused evaluation of how variations in resonator length impact performance metrics.

**Fig. 5** Experimental results: Resonance frequency vs Length of the resonator (L)

Also, taking all resonators and including their simulated data, it was possible to obtain the following results.

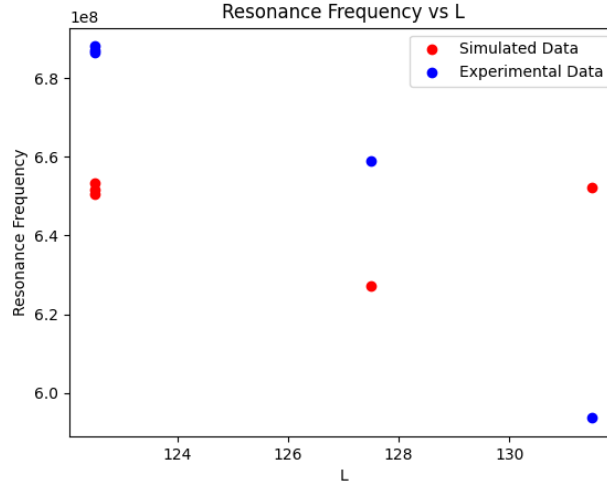


Fig. 6 Experimental and their Simulated results including the 4 covered resonators and the uncovered resonator ($L = 131.0 \text{ mm}$)

The experimental results demonstrate a clear trend: longer resonators exhibit lower resonance frequencies. This behaviour is consistent with the fundamental principle that frequency is inversely proportional to wavelength ($f \propto \frac{1}{\lambda}$). Specifically, a longer resonator supports a longer wavelength, leading to a decrease in resonance frequency.

Regarding the simulation results, this decreasing trend was notable for $L = 122.5 \text{ mm}$ and $L = 127.5 \text{ mm}$. However, for $L = 131.0 \text{ mm}$ the simulation expected a higher resonance frequency.

Comparing and contrasting experimental and simulation results, four resonators exhibited higher resonance frequencies than predicted by their respective simulations. Interestingly, the longest resonator ($L = 131 \text{ mm}$), which featured an uncovered top part, showed a lower resonance frequency than anticipated. This suggests that the physical configuration of the resonator, particularly the uncovered section, may have influenced its electromagnetic properties and contributed to the frequency shift.

To quantify this shift, a graph was generated comparing the differences between the experimental and simulated resonance frequencies (Fig. 7).

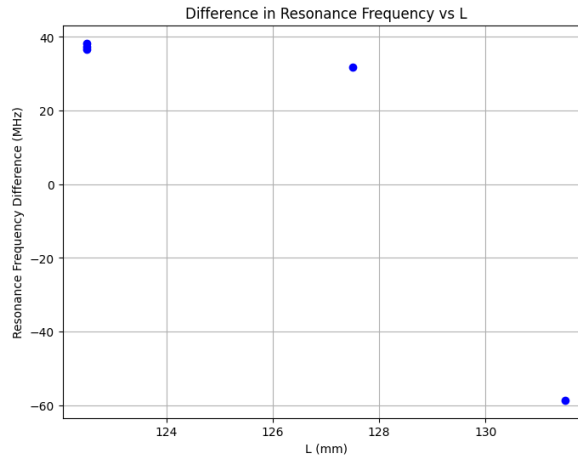


Fig. 7 Resonance Frequency shift between the simulated and experimental

Additionally, a basic statistical analysis was then conducted, with the results summarized in Table 3.

Table 3: Statistics of the Resonance Frequency Shift between experimental and simulation results

Resonance Frequency Shift	Mean [Hz]	Standard Deviation
Including 5 covered and uncovered resonators	17115515.00	± 37927926.53
Only the 4 covered resonators	12034058.18	± 40854051.16

The resonance frequency of experimental data was higher in approximately 12.03 MHz for the covered resonators, and for all resonators was 17.11 [MHz].

3.1 Coupling Factor and Distance between the resonator and its feeding lines (D)

In the subsequent analysis of the Coupling Factor as a function of the distance (D) between the resonator and its feeding lines, we focused exclusively on two resonators that shared identical inductance (L) and width (PW) values. This selection was made to ensure a more consistent and controlled examination, isolating the impact of variations in distance (D) on the coupling factor. The details of the resonators used for this analysis are presented in Table 4.

Table 4: Resonators included in the analysis of Coupling factor (g) vs Distance between the resonator and its feeding line (D)

L	D	PW	PL	Experimental Coupling Factor (g)	Simulation's Coupling Factor (g)
122.5	0.06	0.3	70	0.000473	0.01019
122.5	0.05	0.3	75	0.002791	0.01019

Based on the data in Table 4, we generated the corresponding graph using Python. The resulting plot clearly demonstrates an inverse relationship between the distance (D) and the coupling factor: as the distance between the resonator and its feeding lines increases, the coupling factor decreases.

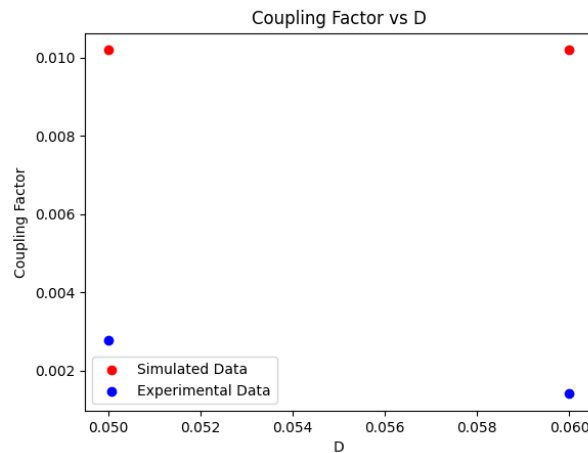


Fig. 8 Coupling factor (g) vs Distance (D) for the 4 covered resonators

The experimental observation aligns with theoretical expectations, as the coupling factor is strongly dependent on the proximity between the resonator and the feeding lines [7]. When the distance increases, the electromagnetic interaction weakens, leading to a reduction in energy transfer efficiency between the resonator and the feeding lines, which is reflected in a lower coupling factor. However, it should be noted that the simulations' data remain constant besides any change in this parameter. Overall, the closer the resonator is to its feeding lines, according to experimental results, the closer it gets to its optimal simulated coupling factor.

Then, a statistical analysis was conducted to evaluate the discrepancy between the expected (simulated) Coupling Factor and the experimentally observed Coupling Factor. The results of this comparison are visually represented in the graph below.

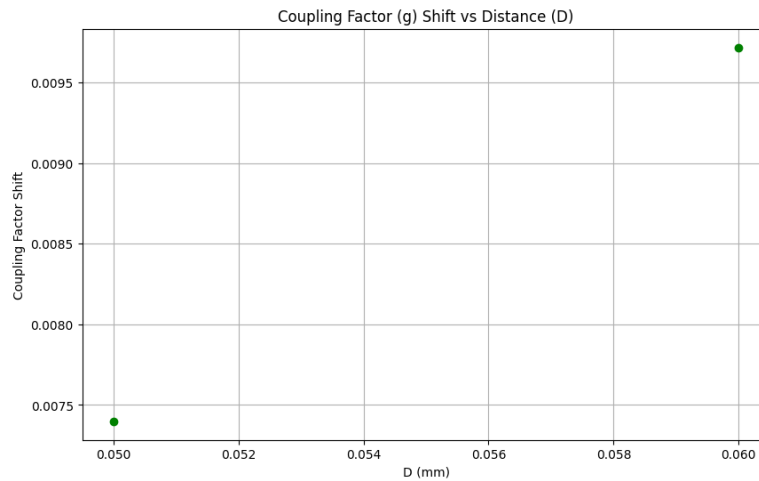


Fig. 9 Coupling factor (g) shift between experimental and simulation results

To provide further insight, table 5 presents the mean values and standard deviations of the differences between the simulated and experimental coupling factors. These metrics offer a quantitative assessment of the variation, highlighting the consistency and accuracy of the experimental results relative to the simulations.

Table 5: Statistics of the Coupling Factor Shift between experimental and simulation results

Coupling Factor Shift	Mean	Standard Deviation
Including 2 covered and uncovered resonators	0.008558	± 0.001159

Overall, in these two covered resonators, that shared common L and PW, but differed in D, the mean Coupling Factor Shift between simulated and experimental results is 0.008558.

4 Conclusions

This study was set out to analyse a series of resonators with varying geometric parameters, assessing their performance through both experimental and simulated data. The primary objective was to evaluate the resonance frequency, coupling factor, and quality factors, while also examining the accuracy of the simulation models against experimental results.

4.1 Experimental Samples

The experimental results revealed that, out of the 13 printed resonators, only 5 exhibited an acceptable quality factor, with values greater than 10, and prominent resonant frequency. The remaining resonators were excluded from analysis due to excessive noise or the absence of a clear resonance frequency, which further suggests issues in the manufacturing process.

Given that the designed flex resonators had an extremely small distance between the resonator and its feeding lines ($D = 0.05$ mm), it is likely that fabrication inaccuracies and imprecision occurred in these critical areas. These fabrication errors are suspected to have caused the observed deviations, as the required precision for such small dimensions may have been difficult to achieve.

As a result, only the 5 resonators with acceptable quality factors were considered for further analysis.

4.2 Simulation and Experimental Results Comparison

Subsequently, the comparison between simulated and experimental results revealed significant discrepancies. Most notably, for the four covered resonators, the experimental resonance frequencies were consistently higher than the simulated predictions, with an average shift of approximately 580.38 [MHz]. In contrast, the uncovered resonator with a length of 131.0 [mm] exhibited a lower experimental resonance frequency compared to the simulated value, with a shift of similar magnitude but in the opposite direction. This suggests that the uncovered section may have introduced additional parasitic effects or altered the boundary conditions in a way that was not captured by the simulation.

Regarding the coupling factor, the experimental data showed a decrease as the distance (D) between the resonator and feeding lines increased, which aligns with theoretical expectations. This inverse relationship is well understood, as increased distance weakens the electromagnetic coupling between the resonator and the feeding lines. However, a noticeable mean shift in the coupling factor between experimental and simulated results was observed. This discrepancy highlights the importance of precise fabrication of resonators to small scales, as required in this project, to minimize such deviations.

4.3 Proposed Improvements

To mitigate these discrepancies, it is recommended to adopt a more precise and accurate fabrication process, specifically tailored for the small scales used in this project. Enhancing the precision in the resonator-feeding line interface could significantly reduce the excessive noise and lack of noticeable resonance frequency observed in most resonators, which appears to stem from fabrication imperfections at these critical junctions.

Furthermore, refining simulation models to more accurately account for real-world mismatches and parasitic effects is essential. By incorporating these factors, the simulations would better reflect the actual conditions, leading to more reliable predictions and a closer alignment between experimental results and theoretical expectations from Pozar [7].

5 List of references

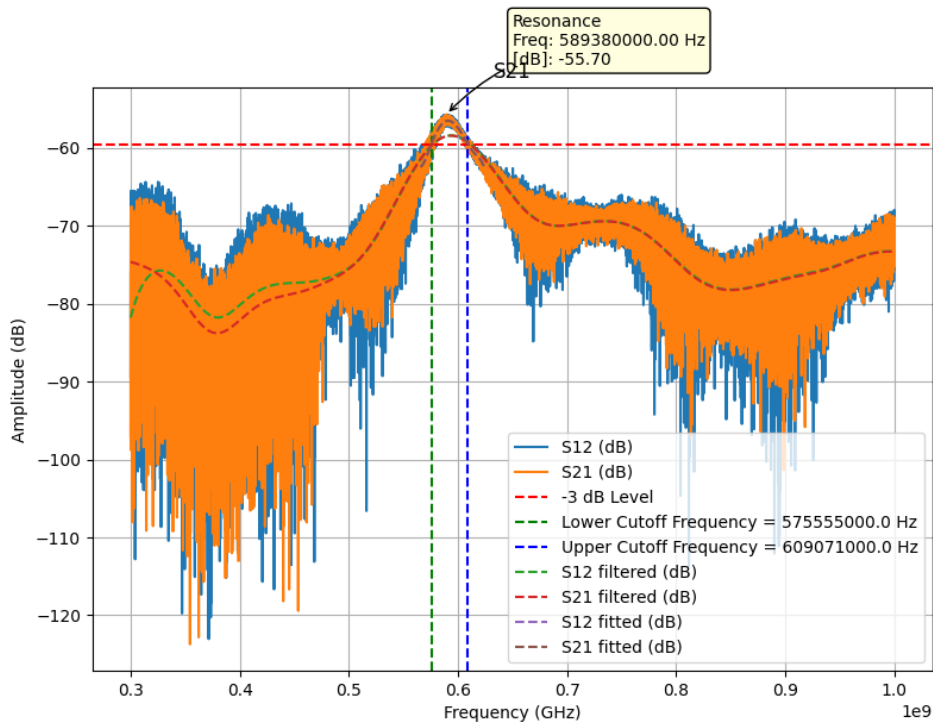
- [1] *The matter-antimatter asymmetry problem*. CERN. (n.d.).
<https://www.home.cern/science/physics/matter-antimatter-asymmetry-problem>
- [2] Hangst, J. (n.d.). *Matter and Antimatter*. YouTube video.
<https://www.youtube.com/watch?v=DACH82j78xY>
- [3] ALPHA Collaboration. (n.d.-a). *ALPHA*. Home | ALPHA Experiment.
<https://alpha.web.cern.ch/>
- [4] ALPHA Collaboration. (n.d.-a). *ALPHA*. Home | ALPHA Experiment.
<https://alpha.web.cern.ch/>
- [5] Amole, C., Ashkezari, M., Baquero-Ruiz, M. et al. Resonant quantum transitions in trapped antihydrogen atoms. *Nature* 483, 439–443 (2012).
<https://doi.org/10.1038/nature10942>
- [6] CERN accelerating science. (n.d.). *Manipulation of antiprotons, positrons and other charged particles*. Penning Trap | ALPHA Experiment.
<https://alpha.web.cern.ch/science/penning-trap>
- [7] Pozar, D. (2012). *Microwave Resonators* (4th ed., pp. 272–316). Book, Wiley.

6 Appendix

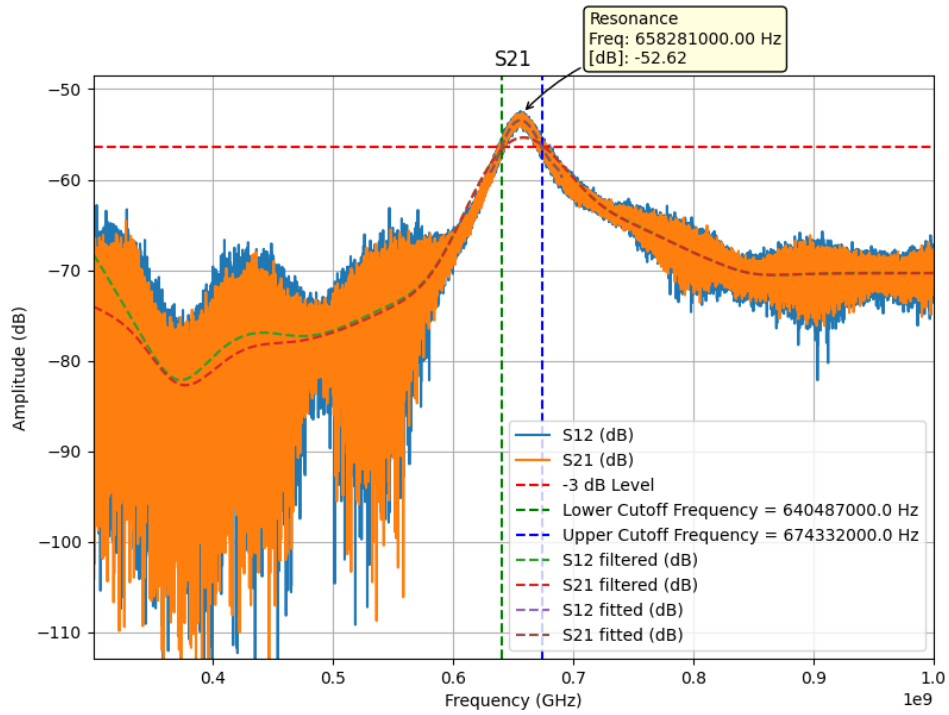
Appendix A: Graphs of the frequency response and evaluation of the 5 final selected resonators

The following plots correspond to the 5 final selected resonator's evaluation and frequency response with the software "Resonator's Analyzer and Plotter". Specifically, the S21 and S22 parameters in decibels are plotted. On top of this, a Butterworth filter is applied to filter the excessive noise. Complementarily, the Lower and Upper Cut-off Frequencies, that were considered for the Quality Factor and Coupling Factor calculation, are visually displayed.

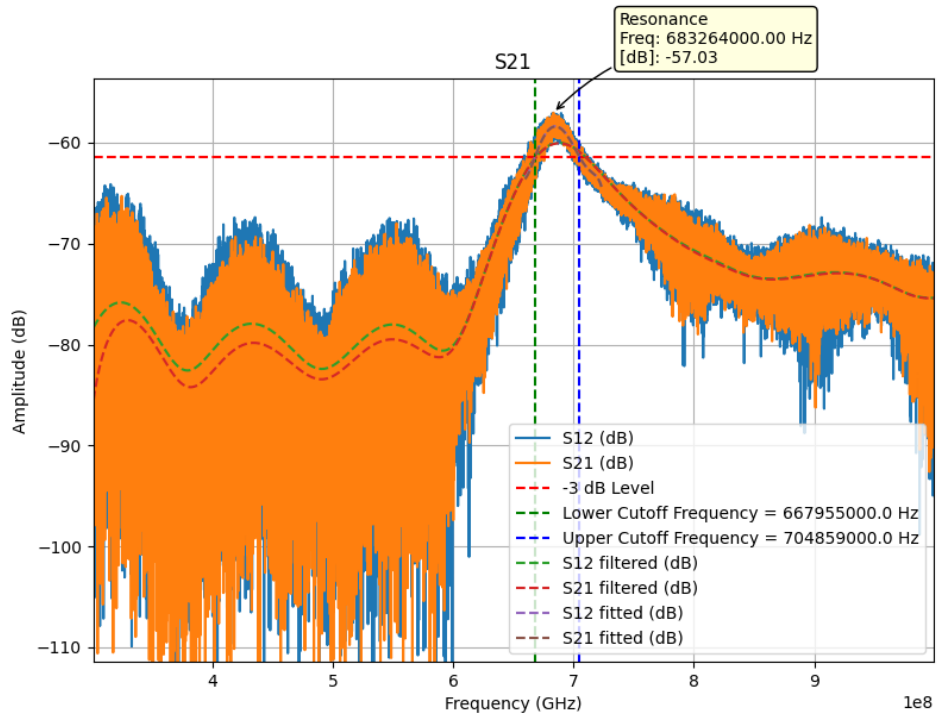
A.1 Resonator with geometric parameters corresponding to $L = 131.5$ mm, $D = 0.05$ mm, $PW = 0.3$ mm, $PL = 70$ mm



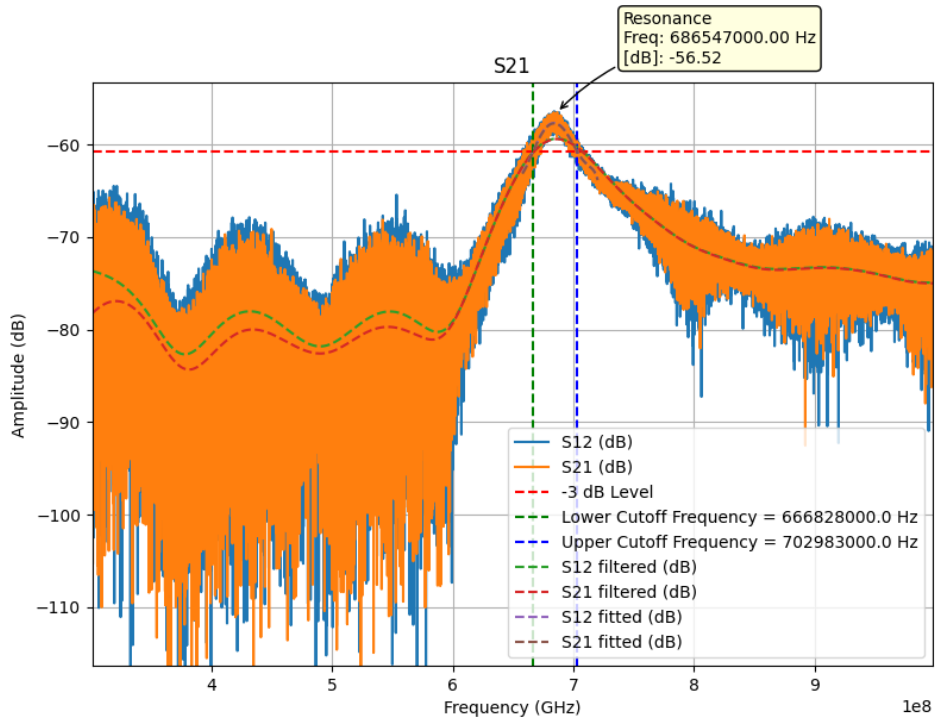
A.2 Resonator with geometric parameters corresponding to $L = 127.5$ mm, $D = 0.05$ mm, $PW = 0.3$ mm, $PL = 70$ mm



A.3 Resonator with geometric parameters corresponding to $L = 122.5$ mm, $D = 0.06$ mm, $PW = 0.3$ mm, $PL = 70$ mm



A.4 Resonator with geometric parameters corresponding to $L = 122.5$ mm, $D = 0.05$ mm, $PW = 0.4$ mm, $PL = 70$ mm



A.5 Resonator with geometric parameters corresponding to $L = 122.5$ mm, $D = 0.05$ mm, $PW = 0.3$ mm, $PL = 75$ mm

